Published by IOP Publishing for Sissa Medialab

Received: *October 7, 2025*
Revised: *January 15, 2026*
Accepted: *March 26, 2026*
Published: *June 1, 2026*

Design and performance evaluation of a novel hybrid ionisation chamber and transmission calorimeter for dose rate independent beam monitoring in UHDR-RT

Samuel Flynn[a,b,*] **Rebecca Habgood**[c,a,d] **Graham Bass**[a] **Anna Subiel**[a,h] **Russell Thomas**[a,e] **Iain Tullis**[f] **Kristoffer Petersson**[f,g] **and Nigel Lee**[a]

[a] *Radiotherapy and Radiation Dosimetry Group, National Physical Laboratory, Hampton Road, Teddington, TW11 0LW, United Kingdom*
[b] *School of Physics and Astronomy, University of Birmingham, Edgbaston Campus, Birmingham, B15 2TT, United Kingdom*
[c] *Department of Physics and Astronomy, University of Manchester, Oxford Road, Manchester, M13 9PL, United Kingdom*
[d] *Christie Medical Physics and Engineering, The Christie NHS Foundation Trust, Manchester, United Kingdom*
[e] *Faculty of Engineering and Physical Sciences, University of Surrey, Stag Hill, Guildford, GU2 7XH, United Kingdom*
[f] *Department of Oncology, Oxford Institute for Radiation Oncology, University of Oxford, Oxford, OX3 7DQ, United Kingdom*
[g] *Department of Haematology, Oncology, and Radiation Physics, Skåne University Hospital, Lund University, Lund, Sweden*
[h] *Medical Physics and Biomedical Engineering, University College London, Gower Street, London WC1E 6BT, United Kingdom*

E-mail: sam.flynn@npl.co.uk

Abstract: **Background**. Ultra-High Dose Rate Radiotherapy (UHDR-RT) is an emerging cancer treatment that delivers radiation at dose rates exceeding 40 Gy/s. While UHDR-RT offers potential therapeutic benefits, accurate dosimetry presents significant challenges. Ionisation chambers, the standard for clinical dosimetry as reference and monitor dosimeters, experience significant ion recombination at high dose rates, reducing measurement accuracy and increasing uncertainty when corrections are applied. In contrast, calorimeters are dose rate independent and potentially more reliable for accurate UHDR-RT dosimetry. However, their slow thermal response limits their use in dynamic beam monitoring.

Purpose. This study investigates whether a hybrid dosimeter, combining an ionisation chamber and two transmission calorimeters, can effectively provide dose-rate independent beam monitoring for

*Corresponding author.

https://doi.org/10.1088/1748-0221/21/06/P06001

both UHDR-RT and conventional radiotherapy (CONV-RT). The goal is to leverage the fast response of ionisation chambers for routine use, while maintaining the dose rate independence of calorimetry for periodic calibrations, to develop a prototype dose rate independent beam monitor.

Methods. The hybrid dosimeter was designed and evaluated using the finite element modelling software, COMSOL, to assess the interactions between the ionisation and calorimeter components. Unwanted electrical and thermal effects were studied, including their impact on electric field distribution, charge collection efficiency, and self-heating effects on calorimetry. After construction, the device was tested at the FLASH Core Facility, University of Oxford, in a 6 MeV UHDR-RT beam. Experimental investigations were conducted under various beam conditions to evaluate performance.

Results. The hybrid dosimeter demonstrated a linear response in both calorimeter cores and the ionisation chamber. Minimal electrical interference was observed in the proximal calorimeter core due to the ionisation process, though this effect was deemed negligible. The ion collection efficiency was measured to be approximately 3% during the highest dose delivery of 6 Gy/pulse (5.4 MGy/s instantaneous dose rate). A Jaffé plot method derived ion recombination factor for a 2 Gy/pulse (1.8 MGy/s instantaneous dose rate) measurement was determined to be 7.84 ± 2.35 ($k = 1$), with a calorimeter derived correction determined to be at least 5.22 ± 0.49 ($k = 1$).

Conclusions. This study successfully demonstrates the feasibility of combining ionisation and calorimetry into a single hybrid dosimeter. The device offers the potential for online beam monitoring with dose rate independence, making it a promising candidate for UHDR-RT dosimetry and further development for clinical use.

Keywords: Dosimetry concepts and apparatus; Radiation monitoring

2026 JINST 21 P06001

Contents

2026 JINST 21 P06001

1 Introduction

1.1 Ultra-High Dose Rate Radiotherapy (UHDR-RT)

Ultra-High Dose Rate Radiotherapy (UHDR-RT) is an innovative cancer treatment technique in which radiation is delivered to a tumour at significantly higher dose rates (> 40 Gy/s) than conventional radiotherapy (CONV-RT), which typically delivers at around 5 Gy per minute [1]. Preclinical studies have demonstrated that UHDR-RT can produce a sparing effect in healthy tissue, commonly referred to as the "FLASH" effect, while maintaining tumour control, particularly when the dose rate exceeds 30–40 Gy/s [2–4]. There is growing research interest in this promising modality, with one clinical trial completed to date (FAST-01) [5], and several other trials currently recruiting or in progress [6–9].

Conventional ionisation chambers, considered the gold standard for dosimetry in both clinical and preclinical settings, are not ideal for UHDR-RT dosimetry due to significant ion recombination at high dose rates [10, 11]. Although correction methods exist to account for ion recombination, they often introduce significant uncertainties. Achieving the ICRU report 24's recommended ±5% uncertainty ($k = 1$) [12] for dose delivery to the tumour is therefore challenging with current dosimetric technologies in UHDR-RT environments, which impedes preclinical and clinical research progress.

1.2 Calorimetry in UHDR-RT

Unlike ionisation chambers, the physical processes underlying calorimetry have been shown to be dose rate independent, making calorimeters well-suited for UHDR-RT dosimetry [13]. Although

heat transfer with the environment is a significant source of uncertainty in calorimetry at CONV-RT, performance improves in UHDR-RT due to the higher dose rates involved. Historically, calorimeters have been confined to use at National Measurement Institutes (NMIs) due to their complexity, but recent challenges in UHDR-RT dosimetry have driven the development of secondary standard calorimeters, expanding their use beyond NMIs [14–16].

The dosimetry challenges presented by UHDR-RT have also prompted the development of novel forms of calorimeter. Previous tests conducted by the National Physical Laboratory using a Transmission Calorimeter at various CONV-RT and UHDR-RT facilities underscored the potential of dose rate independent detectors for beam monitoring [17, 18]. However, the thermal response time of the calorimeter cores, up to several seconds, proved too slow for applications requiring rapid beam interruptions, where microsecond-scale or faster response times may be necessary. While this delay may be acceptable for scenarios involving discrete pulses without the need for immediate feedback, it remains inadequate for many clinical beams, where real-time control is essential.

1.3 Hybrid dosimeter concept

Despite the challenge of ion recombination, ionisation chambers are unlikely to be completely replaced as dosimeters for UHDR-RT due to their stability, adaptability, and compatibility with existing instrumentation and clinical protocols. Their versatility has resulted in a large variety of shapes and geometries, but a typical design consists of two conductive elements separated by an air gap, with materials like aluminium or graphite often used as cathodes or anodes for their conductive properties. To be used as beam monitor instruments, ionisation chambers are required to be as thin as possible, in order to reduce beam attenuation and induced scatter. These transmission chambers require additional correction factors and reconfiguration for UHDR-RT [19, 20], with typical material thicknesses of these beam monitors less than 2.0 mm water equivalent thickness (WET) [21, 22].

This study explores whether two transmission calorimeter cores made from thin aluminium sheets can simultaneously function as an ionisation chamber for beam monitoring, forming a hybrid dosimeter. Such a device could combine the well-established advantages of ionisation chambers — familiarity within clinical settings, ease of use, and fast radiation response — with the dose rate independence of calorimetry. Whilst both novel calorimeters and ionisation chambers have been built before, the authors are unaware of any device that combines both instruments into one form factor. Such a device could establish recombination correction factors within the same device and experimental conditions; and use only the conventional ionisation chamber aspect during beam monitoring. The following sections present the design, simulations, and preliminary experimental evaluations of this novel hybrid dosimeter concept.

2 Method

2.1 Design

The hybrid dosimeter was constructed using two disc-shaped aluminium printed circuit boards (PCBs), each serving as a calorimeter core 45 mm in diameter and approximately 0.6 mm thick. Building the calorimeter cores in this manner allows for established manufacturing techniques to be used, making the design more cost effective. The design was created in FreeCAD [23], and consisted of two parallel cores, separated by a 2 mm surface-to-surface gap. Three fixed supports, made from electrically- and thermally-insulating materials, were used to maintain this separation and ensure

2026 JINST 21 P06001

structural integrity. A 2 mm surface-to-surface gap is larger than typical commercially available monitor chambers and is anticipated to amplify ion recombination effects in UHDR-RT. However, it offers a simplified and easily constructed design, representing a worst-case scenario, that enables initial exploration of the technology concept.

The PCBs (Ventec VT-4B5) were assembled by European Circuits Limited (Beardmore Way, Clydebank Industrial Estate, Clydebank G81 4HT, United Kingdom). Each board contained four thermistors (EPCOS NTC thermistors 10 kΩ at 25°C, $B_{25/100}$ = 4000 ± 3% K), and an integrated circuit (designed by Newbury Electronics Ltd (Faraday Road, London Road Industrial Estate, Newbury RG14 2AD, United Kingdom)) was used to network the thermistors, allowing for the measurement of their average resistance via two electrical connections. Each calorimeter core was connected to an independent Wheatstone Bridge (quarter-bridge type) with a DC bridge supply voltage (V_{BE}) of +10 V.

The PCBs incorporated thermally-conductive dielectric material with a thermal conductivity of 5 W/m·K and a total nominal thickness of 0.6 mm, consisting of an aluminium base of 0.5 mm and a thin dielectric layer of 0.125 mm. Each core was 45 mm in diameter, with thermistors positioned 2.5 mm from the radial edge; on a 5.0 mm wide ring buffer dielectric. A photograph of a PCB core is shown in figure 1. The WET of this hybrid dosimeter in a 6 MeV electron beam is estimated to be 2.3 mm using NIST tabulated data [24]. No additional thermal shielding, other than the aluminised mylar, was incorporated into the design of the prototype.

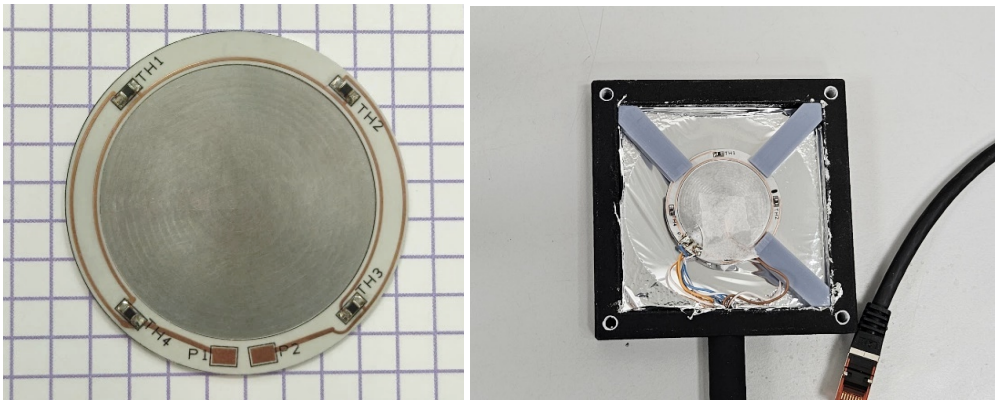

Figure 1. (Left) Photograph of the hybrid dosimeter calorimeter core displaying the thermistor network, (right) photograph of the hybrid dosimeter during construction, highlighting the three supports, wiring, and aluminised Mylar.

2.2 Finite element modelling

The FreeCAD model was imported directly into COMSOL Multiphysics 6.1 [25] as a STEP file, enabling an accurate recreation of the hybrid dosimeter without unnecessary geometric simplifications. A single 3D model was constructed to represent various physics interactions, facilitating detailed simulations across multiple domains. A series of Multiphysics modules were activated to simulate conductive heat transfer, radiative heat transfer, electrical field distributions, and current flow, including: Surface-to-Surface Radiation, Heat Transfer in Solids and Fluids (coupled with surface-to-surface radiation), and Electric Currents, which was integrated with Heat Transfer in Solids and Fluids using the Electromagnetic Heating Multiphysics module.

2026 JINST 21 P06001

The hybrid dosimeter is intended to be positioned in a radiation beamline such that the core discs are perpendicular to the beam axis. The proximal aluminium core (the core nearest to the radiation source) was assigned a high tension (HT) of −200 V, while the distal aluminium core was grounded at 0 V. The circuitry on the front and rear faces of the calorimeter was represented by a thin copper halo centred around the thermistors (inner radius 19.5 mm, outer radius 20.5 mm). Although the actual electrical potential of the temperature circuit would vary between +5 V and 0 V at different points on the PCB, this was uniformly modelled as +5 V throughout to study the worst-case scenario. This HT value was chosen semi-arbitrarily to balance performance concerns, as the device was a prototype. The voltage was mostly kept low to avoid potential issues with electrical sparking and breakdown of the 3D printed supports.

The outer case of the dosimeter was included in the COMSOL model. This outer casing was fixed as a stationary heat source, representing the ambient laboratory temperature of 20 degrees Celsius. This setup approximated the planned experimental studies at the University of Oxford, which utilised a controlled temperature enclosure, and allowed for the investigation of heat flow within the hybrid dosimeter to be studied.

In addition to reporting average temperatures, the voxelised thermistors within the model were configured to function as small heaters, dissipating power according to Ohm's Law:

$$P = \frac{\left(\frac{V_{\mathrm{BE}}}{2}\right)^2}{R_0}$$

For a V_{BE} of 10 V, this results in a nominal constant heater output of 2.5 milliwatts.

Six copper wires (two for each calorimeter circuit — one for HT and one for the collector), with a diameter of 0.25 mm, were modelled to connect the relevant components in COMSOL. These wires were linked to a fixed boundary condition of 20 degrees Celsius, located 10 cm from the centre of the dosimeter, to represent heat transfer through the wires. This modelling aimed to determine the worst-case scenario for conductive heat transfer through the wiring.

2.3 Construction

The FreeCAD model was exported as STL files for 3D printing. The outer case of the hybrid dosimeter was printed using glass-embedded nylon via selective laser sintering (SLS). This was chosen due to its rigidity and suitability for functional prototyping. Internal supports, used to separate the calorimeters, were 3D printed with AnyCubic Plant-Based UV Resin (grey) due to its ability to manufacture the 0.6 mm slits, its low thermal conductivity (estimated to be approximately 0.1 W/m·K) and high electrical resistivity (estimated to be greater than $1 \times 10^{14}\,\Omega\cdot$ cm).

As shown in figure 1, the two calorimeter cores were held in place by three supports extending to three corresponding corners of the square outer case. The fourth corner of the outer case was intentionally left empty to accommodate cabling. Only three supports were necessary for rigidity, as a fourth would have increased thermal conductivity without providing significant additional structural support.

The interior volume was lined with aluminised mylar to minimise environmental thermal interference, and the dielectric in the centre of each core was machined away to reduce WET.

The signal and bias voltages were sent over CAT6 ethernet cable and an RJ45 interface on the detector. This wiring configuration was chosen for its paired correlated signals to minimise electrical noise.

2026 JINST 21 P06001

Internally, the HT and collector electrodes were connected using standard copper wire secured to the exposed aluminium surfaces with non-conductive adhesive tape. The assembled dosimeter was sealed with electrical tape to reduce airflow and prevent accidental contact with the ionisation chamber components. The Wheatstone bridge-out-of-balance voltage for each calorimeter core circuit was measured by a Keithley 6500 digital Multimeter (DMM). The calibration of the bridge-out-of-balance voltage against temperature was performed in an environmental chamber, traceable to the NPL primary standard for temperature, across a temperature range of 18 to 30°C.

A 6517B Keithley Electrometer supplied the HT and measured charge, while a bespoke Python script synchronised the readout of all instruments. For ease of transport, the RJ45 cable extending from the hybrid dosimeter was limited to 30 cm. A commercial 20 m Category 6 RJ45 extension cable was used during in-beam experiments to connect the dosimeter in the radiation exposure room to the instrumentation in the control room. The temperature calibration was performed with this extension cable fitted but without HT activation.

The DMMs sampled at approximately 10 Hz, while the 6517B Electrometer operated at about 7 Hz. The Python-based data acquisition software issued simultaneous read commands and waited for all instruments to respond before initiating the next cycle, resulting in an effective overall sampling rate of approximately 7 Hz. No averaging or filtering was applied to any of the recorded signals.

2.4 Experimental evaluation at the University of Oxford

The hybrid dosimeter was tested at the FLASH Core Facility, University of Oxford [26], using a modified clinical linear accelerator, shown in figure 2. For uniform, homogenous beams, the linear accelerator can deliver up to ~ 6 Gy/pulse (~ 3.4 µs pulse length, 300 Hz pulse repetition frequency) to investigate the performance in UHDR-RT, as well as CONV-RT and lower dose rates (at 25 Hz pulse repetition frequency). The exposure area is situated on an optical table within a controlled "greenhouse" environment, which facilitates repeatable measurement setups and minimises environmental temperature fluctuations that could introduce thermal noise.

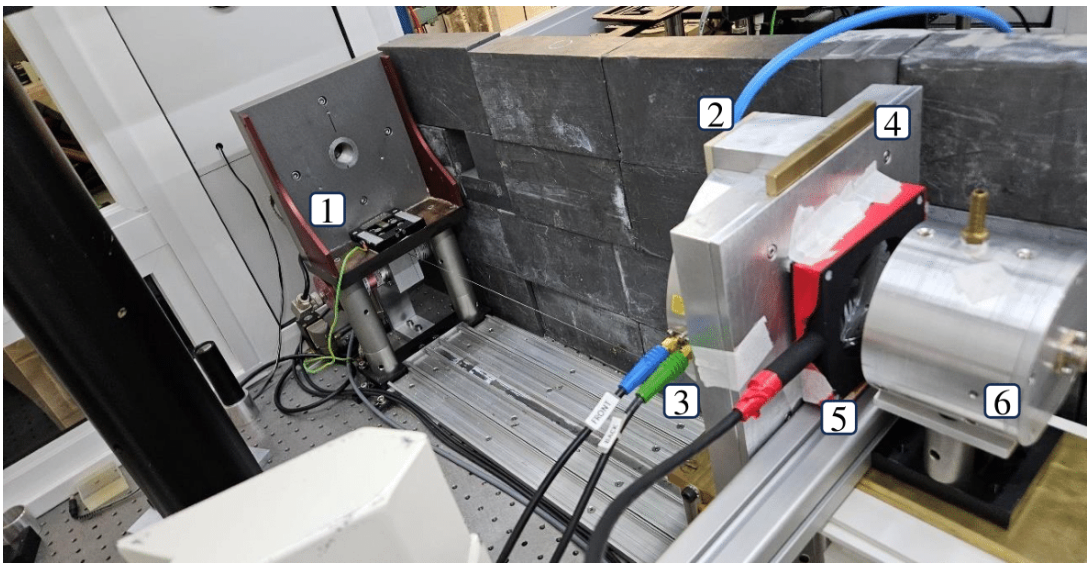

Figure 2. Setup of the Hybrid Dosimeter. Legend key: 1 — Exit Nozzle, 2 — Ionisation Chamber, 3 – Energy Monitor, 4 — Brass collimator insert, 5 — Hybrid Dosimeter, 6 — Faraday Cup (beam dump).

2026 JINST 21 P06001

Throughout this study, a 6 MeV electron beam was used at 300 Hz pulse repetition frequency (PRF). The hybrid dosimeter was positioned at the local reference conditions, with a 6 mm thick brass collimator with a 35 mm aperture applied to shape the beam. In this setup, the dosimeter operated as a dose-area-product instrument in both calorimetry and ionisation chamber modes. A Faraday cup was placed behind the dosimeter to act as a beam dump. The dosimeter's response was compared to an energy monitor [26] and an Advanced Markus ionisation chamber placed in the beam halo.

For calorimetry analysis, temperature data were fitted with a second-order polynomial after excluding the period of internal heat flow. Ionisation chamber data, which recorded accumulated charge over time, were processed using the same software but with a linear fit rather than a quadratic one.

2026 JINST 21 P06001

3 Results

3.1 COMSOL simulations

3.1.1 Thermal performance

The COMSOL simulations showed that in the enclosed environment with a constant 5 V supply to the 10 kΩ thermistors and a −200 V HT applied, the temperature of the calorimeter cores stabilise at approximately 336 mK above ambient. This heat is transferred to the aluminium core through the dielectric material, where it dissipates via air, the 3D-printed supports, and the copper wiring.

The temperature distribution for individual components of the simulated hybrid dosimeter at equilibrium is shown in table 1. The thermistors self-heat, raising their temperature by approximately 490 mK above ambient. Since the precise geometry of the thermistors is not well defined, the electrical self-heating was uniformly distributed across voxels in COMSOL rather than applied to a small heating element. Differences between the cores are attributed to numerical noise.

The low standard deviations in temperature across both cores indicate a uniform temperature distribution, an important characteristic for accurate calorimetry. The fact that each core is asymmetrically-supported at three points introduced the possibility of non-uniform temperature distribution, but this concern was not reflected in the simulation results, as shown in figure 3.

Table 1. Average temperature above ambient for components of the hybrid dosimeter based on COMSOL simulations.

Component	Temperature above Ambient (mK)		Number of Voxels
	Average	Standard Deviation ($k = 1$)	
Proximal Calorimeter Core Body	335.7	1.6	1008
Proximal Calorimeter Dielectric	336.0	3.3	1365
Proximal Calorimeter Thermistors	490.4	150.1	33
Distal Calorimeter Core Body	336.1	1.5	973
Distal Calorimeter Dielectric	336.3	3.3	1377
Distal Calorimeter Thermistors	492.6	148.9	34
3D printed Supports	186.3	157.9	1845

Figure 3 shows temperature distributions from the COMSOL simulations. In the top plot, due to their size, the thermistors are not visible.

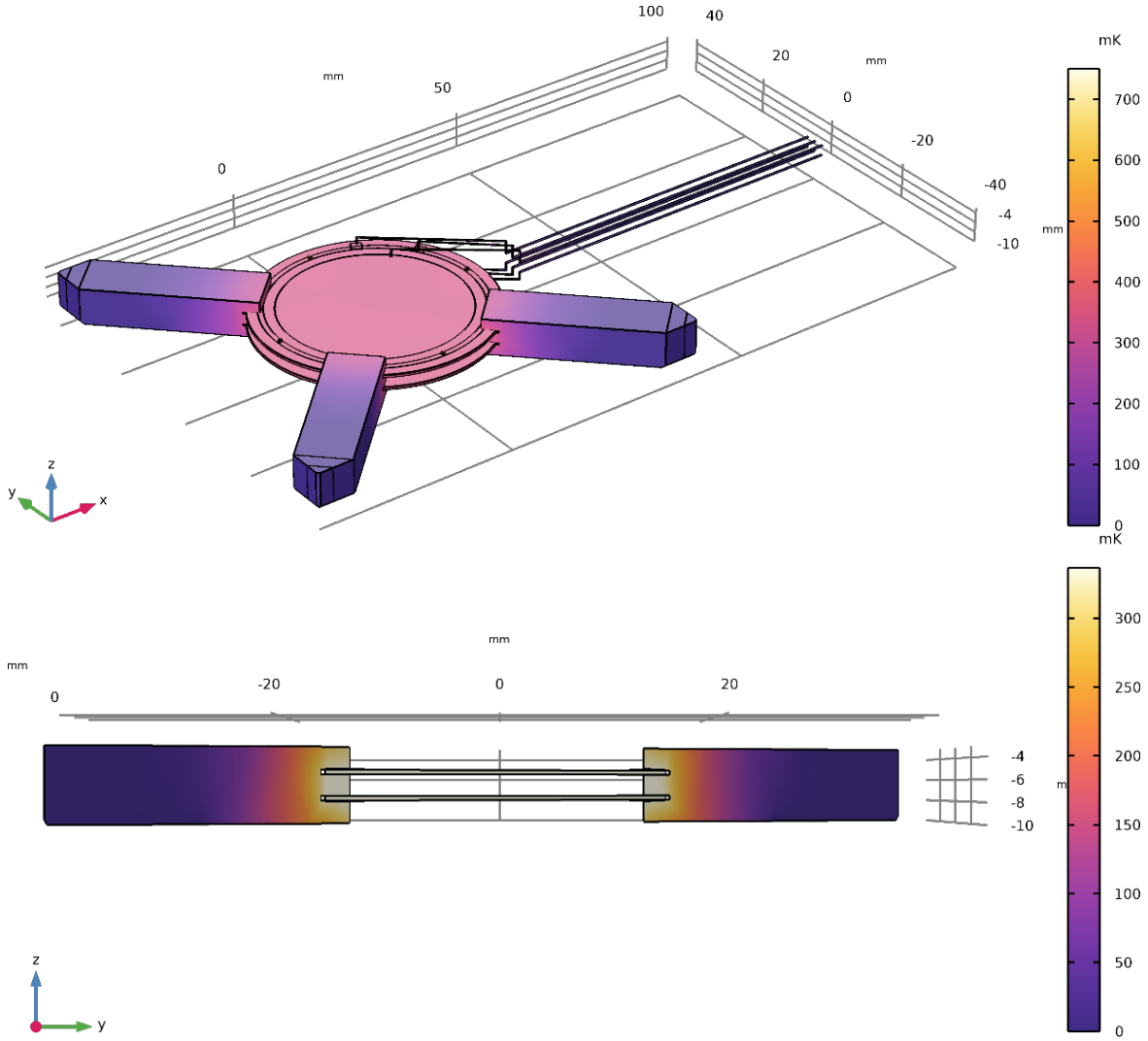

Figure 3. Equilibrium heat flow simulations for the hybrid dosimeter. (Top) Isometric view. (Bottom) Diagonal cross section view, through the two 3D printed supports.

To investigate conductive heat loss of the Hybrid Dosimeter, heat transfer through the supports and the copper wiring was selectively enabled/disabled. These are described in table 2. The amount of heat loss predicted from both of these methods is nominally the same, reducing the equilibrium temperature of the proximal core and thermistor by approximately 18% each.

Table 2. Investigation of the ambient thermal temperature rise for the proximal core's thermistors and core body, for −200 V HT, and +10 V V_{BE}.

	Support: Enabled	**Support: Disabled**
Wire: Enabled	Thermistor: 487.26 mK Core body: 338.61 mK	Thermistor 560.40 mK Core body: 412.60 mK
Wire: Disabled	Thermistor: 554.12 mK Core body: 406.00 mK	Thermistor: 664.84 mK Core body: 517.95 mK

2026 JINST 21 P06001

By systematically varying heating sources within the model, it was also determined that the average temperature of the thermistors increases by only 1.6 mK above ambient when −200 V HT and 0 V V_{BE} are applied (a condition representing HT only without any calorimetry circuitry excited). This relationship is observed to be nominally linear between 0 and −1000 V HT, with a maximum electrical heating of less than 6 mK. This minimal temperature rise is well within the noise floor of the COMSOL model, indicating that the ionisation chamber's operation does not adversely affect the calorimeter's functionality. Additionally, any heat generated within the 3D-printed supports due to electrical heating remains negligible.

While variations in the bulk resistance of the 3D-printed support could affect temperature, the extent of such changes would need to be significant to have a detrimental impact on calorimeter performance. This reinforces the conclusion that the ionisation chamber and calorimeter can function simultaneously without compromising measurement accuracy.

In contrast, when adjusting the V_{BE} while keeping the HT at 0 V, a quadratic relationship between temperature and excitation voltage is observed, consistent with the V^2 dependence previously discussed in section 2.2. These relationships are illustrated in figure 4, further emphasising the importance of excitation voltage on thermal performance while establishing that ionisation HT does not negatively impact the calorimeter's functionality.

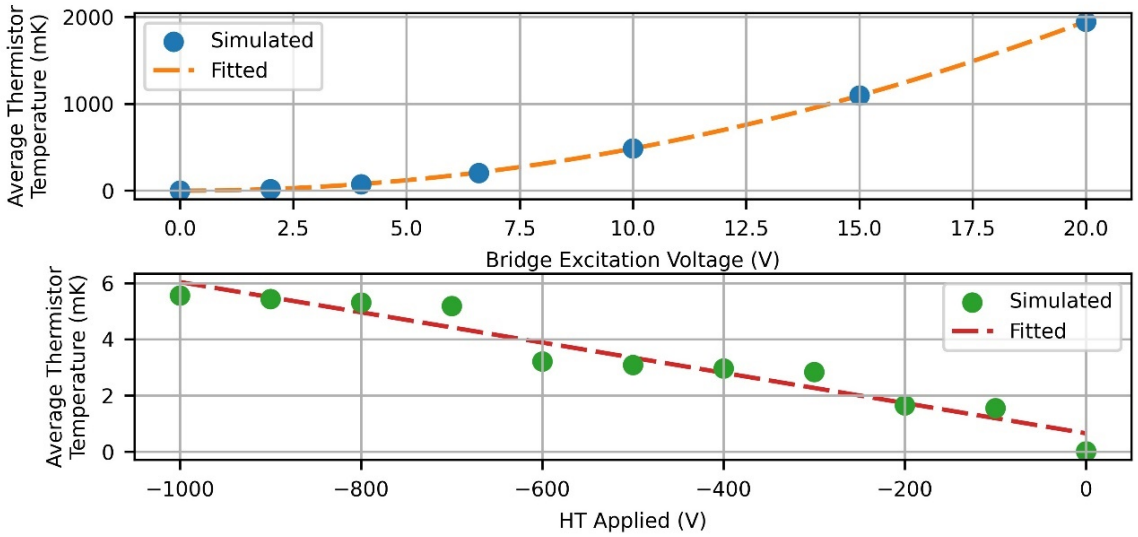

Figure 4. Comparative analysis of heating contributions in the hybrid dosimeter.

3.1.2 Electrical field interference

The COMSOL simulations indicate that ionised air near the proximal calorimeter can interfere with both the temperature sensing circuitry and the current collection circuitry of the ionisation chambers. This interference is driven by the large potential difference in this region (−200 V for the ionisation chambers versus +5 V for the sensing thermistors), which can create localised "dead zones" where electron-ion pairs are not collected within the chamber's cathode-anode circuit. Within these zones, ionic drift towards the calorimeter rather than the chamber ground may occur, leading to short voltage spikes on the calorimetry circuit. These spikes are expected to occur on a very short timescale;

2026 JINST 21 P06001

typically nanoseconds to microseconds; and could momentarily perturb the temperature measurement signal, though not enough to cause sustained error.

The region of potential interference extends approximately 2.5 mm on either side of the thermistor. The distal calorimeter, acting as the grounded collector, experiences a similar effect on a smaller scale due to its lower potential difference (5 V to 0 V ground). Overall, COMSOL results suggest that while these transient effects can occur intermittently during UHDR-RT, their impact on ionometry remains minimal because the primary collection volume between the two cores is unaffected.

As shown in figure 5, the electric field inside the volume is relatively uniform. However, the intentional absence of a guard ring (to simplify the design), which is typically used in ionisation chambers, causes noticeable bowing of the electric field beyond the edges of the calorimeter cores. For beam sizes $\leq$ 35 mm FWHM, the calorimeter sensing circuit is expected to operate normally. However, for fields > 45 mm FWHM, the ionisation chamber's response becomes less predictable. Since the intended use of the device is that of a dose-area-product instrument, the measured signal is proportional to beam size. Based on these considerations, the initial experimental dosimetry studies were limited to 35 mm fields.

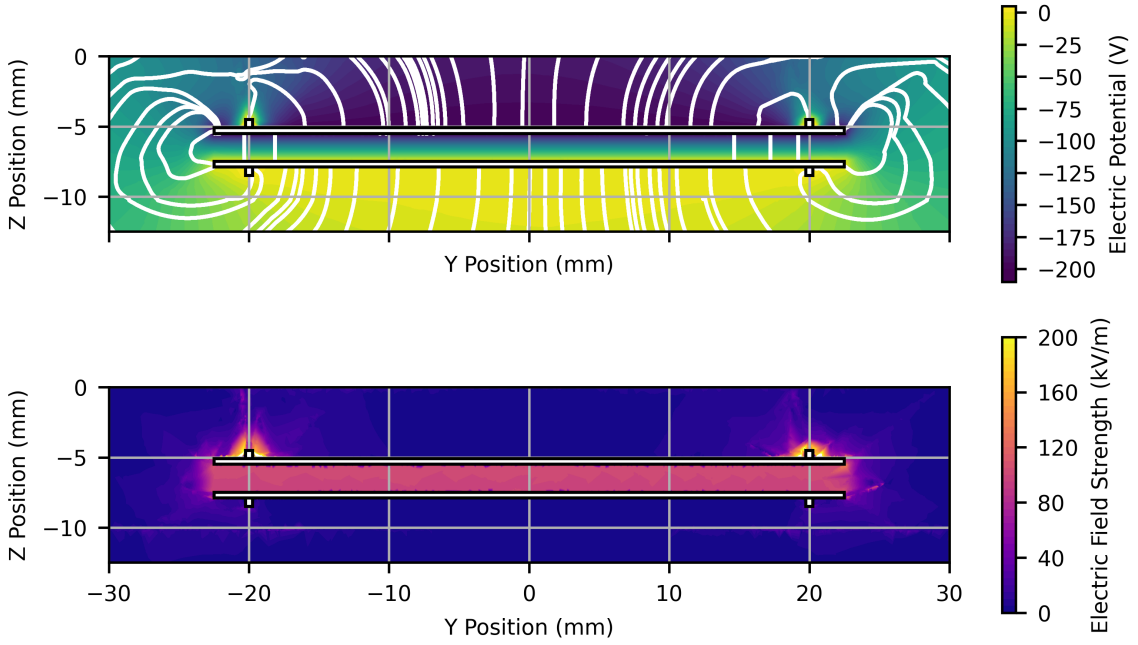

Figure 5. Electric field simulations of the hybrid dosimeter, showing (top) electric potential with field streamlines and (bottom) electric field strength distribution.

3.2 Experimental results

3.2.1 Dose response

The response of the hybrid dosimeter to a 10 Gy UHDR-RT delivery, delivered in five 2 Gy pulses (300 Hz PRF, 600 Gy/s average dose rate, 1.8 MGy/s maximum instantaneous dose rate) can be seen in figure 6. For the ionisation chamber there is observed to be a near instantaneous change in the current recorded, occurring in less than 0.1 s (the sampling resolution of the electrometer), whereas

2026 JINST 21 P06001

the calorimeter cores take approximately 3 s to reach peak thermal response. The proximal and distal calorimeter (with independent readout systems) follow a similar thermal loss pattern.

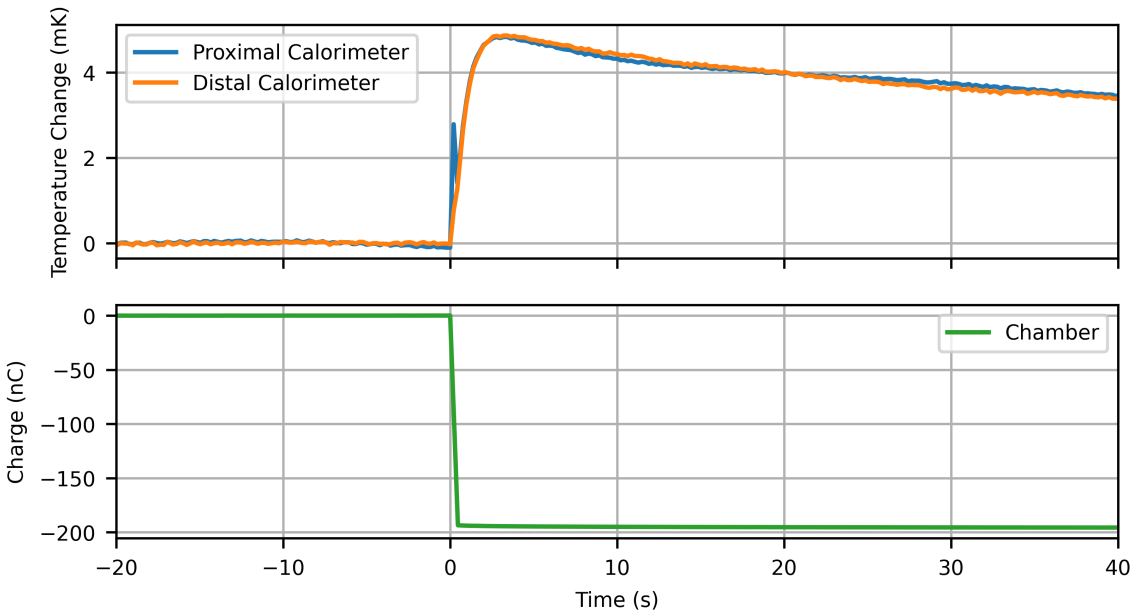

Figure 6. Instantaneous response of the Hybrid Dosimeter to a 10 Gy UHDR-RT delivery (2 Gy/pulse, 300 Hz PRF), showing the two calorimeters' temperature response (Top) and the ionisation chamber's electrical response (Bottom).

Figure 6 shows a transient electrical spike observed in the proximal calorimeter. Electrical simulations, as discussed in section 3.1.2, indicated that such transient behaviour could occur due to electric field interference between the ionometric and calorimetric components. The leakage current of the ionisation chamber was measured to be approximately 0.5 nA with −200 V HT applied, which was corrected prior to analysis of the charge deposited.

The spike is attributed to electrical noise, caused by this transient interference during radiation delivery. The agreement of the two calorimeters after the transient spike is indicative that it does not produce any longer-term effects. Traditional calorimeter fitting algorithms do not account for the temperature response during radiation delivery and heat flow, so this brief fluctuation is not included during the fitting process. Consequently, as this spike is momentary, it is not believed to impact the overall performance of the calorimeter.

3.2.2 Linearity

Figure 7 illustrates the response of the various calorimeter components to a variable number of UHDR-RT 2 Gy pulses (1.8 MGy/s instantaneous dose rate), assessing the linearity of the device over a dose range of 2 to 100 Gy. To allow for heat dissipation, there was a conservative gap of 120 seconds between each irradiation. The pulses were administered in a non-sequential order (determined randomly) to mitigate any potential trends, with only a single exposure conducted at each dose point. The results indicate that both the calorimeters and the ionisation chamber exhibit excellent linearity, with all components achieving an R^2 value greater than 0.999.

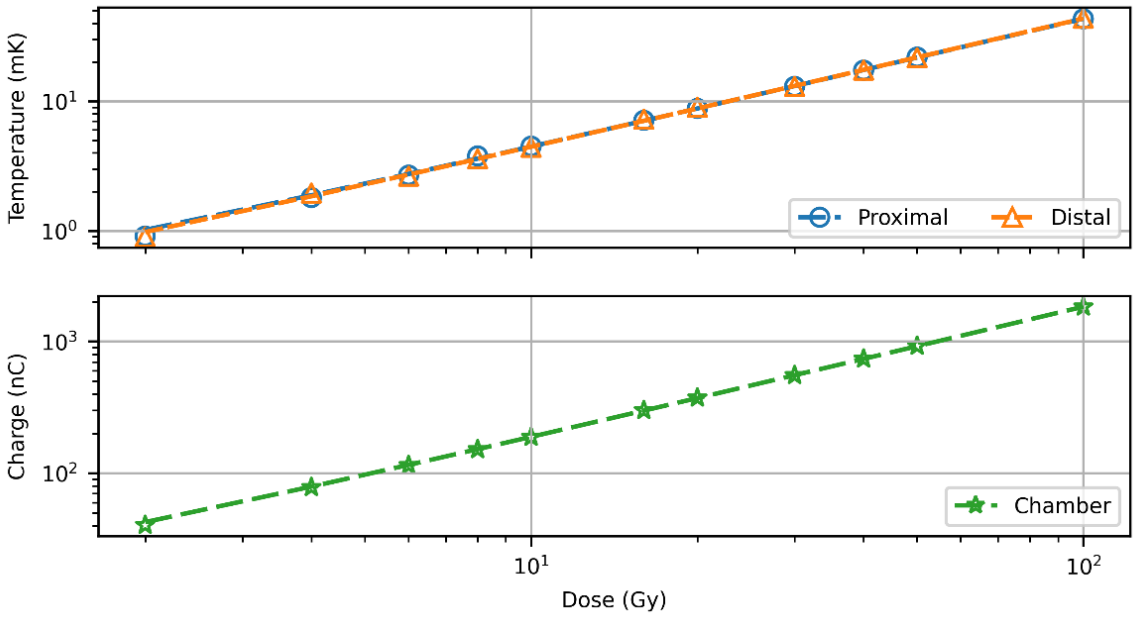

Figure 7. (Top) Logarithmic scale showing the temperature response of the proximal and distal calorimeter cores. (Bottom) Logarithmic scale depicting the absolute charge response of the ionisation chamber. Please note that the charge collected was negative but has been normalised for clarity in this plot.

3.2.3 HT study

Figure 8 illustrates the ionisation chamber's response to 10 Gy deliveries, administered as five UHDR-RT 2 Gy pulses, across different HT voltages. Before recording these measurements, a cumulative pre-dose of 100 Gy (fifty 2 Gy pulses) was delivered at UHDR-RT dose rates to stabilise the chamber after each voltage change. This pre-dose, though much higher than typical clinical doses, was applied to ensure the chamber had fully stabilised. This approach was chosen to mitigate any transient effects and encourage consistent performance in the prototype chamber.

The charge-polarising voltage response of the hybrid dosimeter to 2 Gy/pulses is shown in figure 8 (top), with a Jaffé plot shown below. The y-intercept ($1/k_s$) of the linear fit is 0.128 ± 0.04 ($k = 1$), resulting in an ion recombination factor of 7.84 ± 2.35 ($k = 1$), considerably greater than correction factors in conventional radiotherapy and also with an unacceptably high uncertainty.

The polarity correction factor k_p is calculated as $k_p = \frac{|M_+|+|M_-|}{2|M_{\text{ref}}|}$ where M_+ and M_- are the readings at equal positive and negative bias voltages (± 200 V), and M_{ref} is the reading at the reference polarity (here, -200 V). For the 2 Gy per pulse, collimated 35 mm diameter beam, k_p was determined to be 1.013 ± 0.022 ($k = 1$), which is notably higher than that of standard ionisation chambers. This discrepancy can be attributed to electric field interference caused by the proximity of the calorimeter circuitry and the absence of a guard ring, which typically helps maintain a uniform electric field within ionisation chambers.

3.2.4 Dose rate study

When delivering the same nominal dose (10 Gy) at the lowest relevant dose rate available without retuning the machine (5 mGy/pulse, 300 Hz PRF, 1.5 Gy/second average dose rate, 1.5 kGy/s maximum

2026 JINST 21 P06001

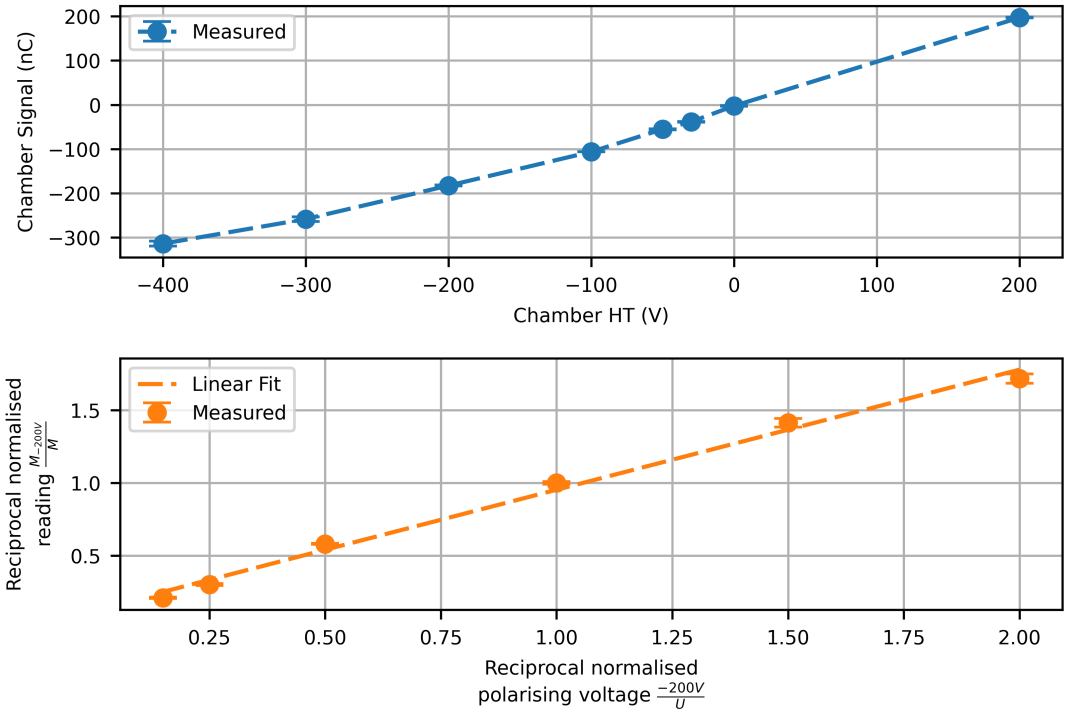

Figure 8. (Top) Response of the ionisation chamber to different HT voltages. (Bottom) Jaffé plot of chamber response.

instantaneous dose rate) it is observed that the electrical spike in the proximal calorimeter signal, associated with ionometry interference, is more pronounced (figure 9).

This behaviour is consistent with the expected effects of ion recombination being less pronounced at low dose rate. However, as shown previously, there is no observable difference in the overall performance of the two calorimeters. In the irradiation shown in figure 9, both the ionisation chamber and calorimeter plots show a change in gradient at approximately 3 seconds after the start of the beam, likely due to the linear accelerator warming up during the delivery.

The linear accelerator was then set to deliver a nominal dose of 10 Gy at various dose rates: 5 mGy/pulse, 130 mGy/pulse, 300 mGy/pulse, 2 Gy/pulse, and the machine's maximum dose per pulse of 6 Gy/pulse in this configuration (resulting in a total of 12 Gy, normalised to 10 Gy for comparison). For consistency, the linear accelerator PRF was fixed at 300 Hz. The relative responses of the proximal calorimeter, distal calorimeter, and ionisation chamber were evaluated across these dose rates, with each dataset being normalised to the 5 mGy/pulse delivery to facilitate comparison across the different conditions. This data is shown in figure 10.

It appears that for both calorimeters, the relative signal decreases as the dose per pulse increases. Additionally, the calorimeter's response for 300 mGy/pulse is approximately 20% lower than the 13 mGy/pulse or 2 Gy/pulse measurements). As data from both calorimeters is independently acquired, this variation and trend were attributed to the tuning of the linear accelerator against the energy monitor as this is only calibrated against EBT-XD radiochromic film at UHDR-RT (6 Gy/pulse 300 Hz PRF) and CONV-RT (5 mGy/pulse at 25 Hz PRF). Non-standard dose per pulses configurations required interpolation of linear accelerator settings which may have resulted in errors in dose delivery.

2026 JINST 21 P06001

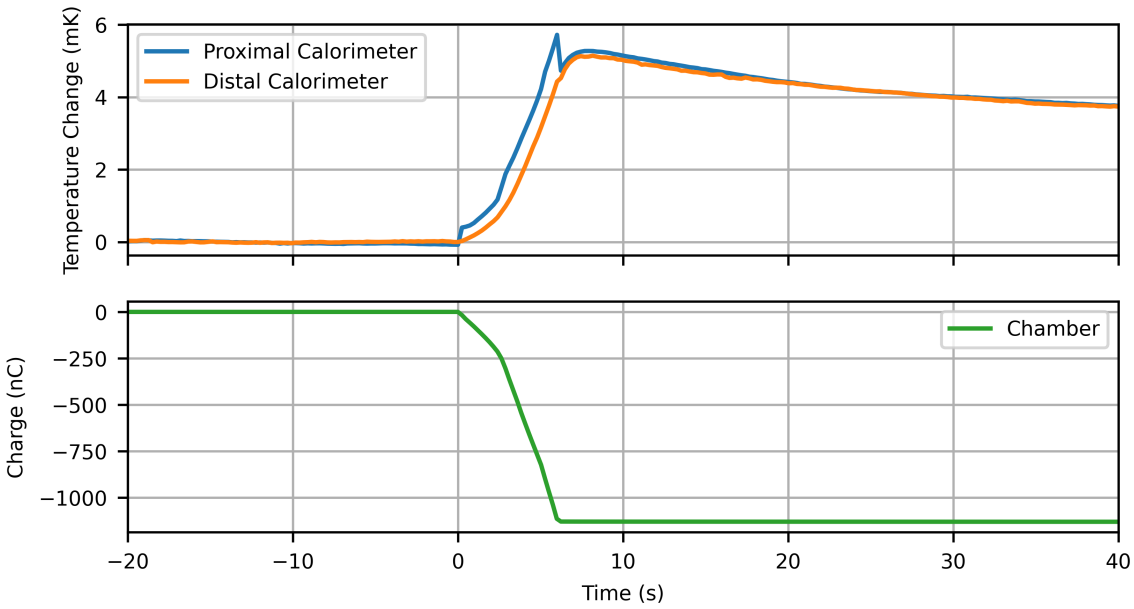

Figure 9. Instantaneous response of the Hybrid Dosimeter to a 10 Gy non-UHDR-RT delivery (5 mGy/pulse, 300 Hz PRF).

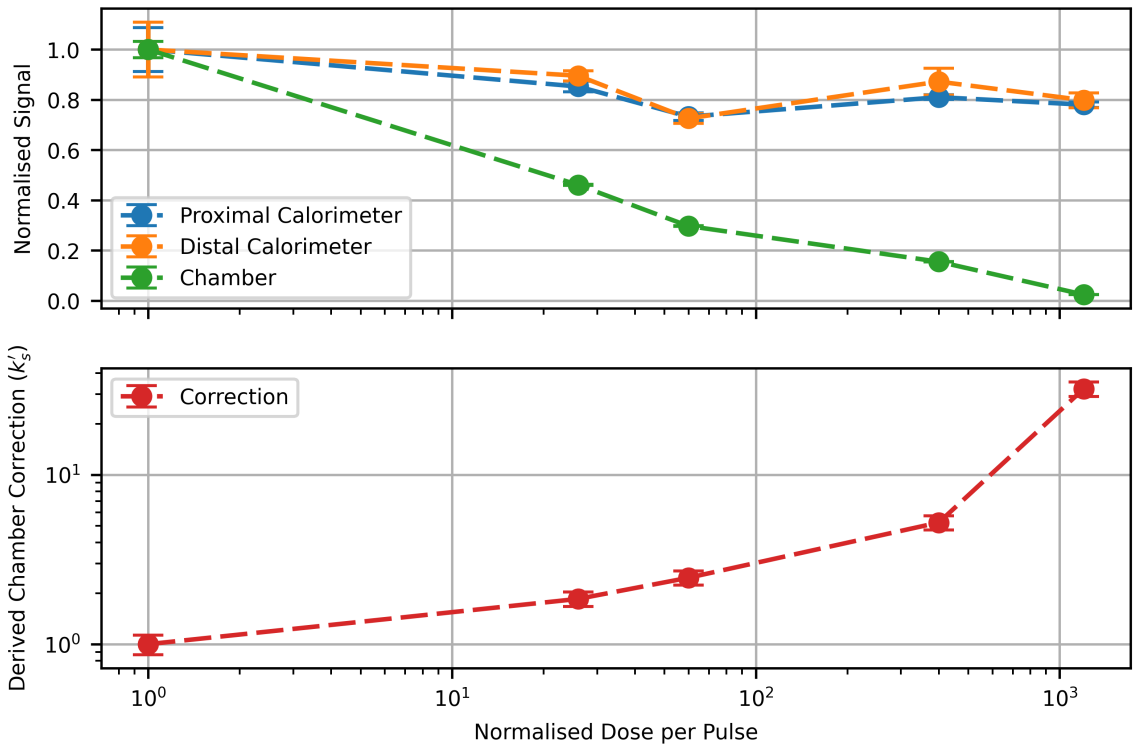

Figure 10. (Top) Comparison of the relative signal response between the proximal and distal calorimeters (temperature rise) and the ionisation chamber (collected charge), normalised to the 5 mGy/pulse delivery. (Bottom) Proximal calorimeter-derived ion recombination correction factor.

Alternatively, the lack of adequate thermal modelling of the calorimeters' heat evolution may have resulted in insufficient correction for thermal losses to the environment. No heat-transfer correction factor (k_{th}) was applied to this dataset, which it would be as is standard for primary-standard calorimetry but not necessarily for secondary-standard instruments. The delivery of the lowest dose rate (5 mGy/pulse, 300 Hz PRF, or 1.5 Gy/s) takes approximately 6.7 seconds to deliver the target dose, compared to just 6.7 ms for the shortest beam duration. This extended exposure time could amplify thermal losses, which may not be accounted for by the current extrapolation-based temperature-fitting algorithm.

It can be observed that the hybrid dosimeter ionisation chamber experiences a significant reduction in charge collection efficiency as a function of dose per pulse, with only 15.5% of the charge collected at 2 Gy/pulse compared to 5 mGy/pulse. At the maximum 6 Gy/pulse, this trend continues, with the ionisation chamber collecting approximately 3% of the CONV-RT signal.

By assuming that the 5 mGy/pulse investigation represents 100% efficiency, it is possible to determine a calorimeter-derived ion recombination correction factor (k'_s) of the higher dose rates by comparing the ratio of the calorimeter and ionisation signals. These are calculated to be 1.85 ± 0.18 ($k = 1$), 2.47 ± 0.24 ($k = 1$), 5.22 ± 0.49 ($k = 1$), and 32.2 ± 2.4 ($k = 1$) for 13 mGy/pulse, 300 mGy/pulse, 2 Gy/pulse, and 6 Gy/pulse respectively. The derived ion recombination for the 2 Gy/pulse configuration is less than that determined using the Jaffé plot method, as it does not inherit any ion recombination from the 5 mGy/pulse measurement, however there is an overlap within the calculated Type A uncertainties.

4 Discussion

This study investigated and compared the response of a novel hybrid dosimeter against equipment used for UHDR-RT research at a preclinical research centre. As a preliminary exploration of technology, it does not offer full comparison to state-of-the-art UHDR-RT equipment such as the PTW flashDiamond diode detector [27], or an ultra-thin ionisation reference chamber [28]. Known improvements to ionisation chambers such as a guard ring were not incorporated as this work was limited to a feasibility study of basic design concepts.

Although recent studies have indicated that radiochromic film may exhibit dose-rate dependence at very high instantaneous dose rates, potentially overestimating dose by up to 10% under extreme conditions [29–31], independent validation of the dosimetry was previously performed using alanine. This comparison revealed only a 1.6% difference between a 5 Gy/pulse delivery and a 5 mGy/pulse delivery, which is well within the expected uncertainty for film-based dosimetry. These findings suggest that while film behaviour at ultra-high dose rates warrants continued investigation, the observed discrepancy in this study is more likely attributable to limitations in thermal modelling and correction rather than film calibration alone. Future work will incorporate improved thermal modelling of the calorimeter system and apply heat-transfer correction factors, alongside independent dose verification using multiple modalities under UHDR conditions. In addition, thermal modelling could be used to improve the design the of a future hybrid dosimeter to minimise thermal contamination and improve overall measurement accuracy.

The ability of the hybrid dosimeter to transfer an ion recombination correction factor for its chamber from one dose-rate to another via the calorimeter was partially evaluated in this study, showing overlap of uncertainties between the conventional voltage determined method and calorimetry derived method.

2026 JINST 21 P06001

Large uncertainties, owing to the prototype nature of the device, are observed hindering detailed comparison but highlighting the technological feasibility. Additionally, as the calorimeter-derived ion recombination factor uses the 5 mGy/pulse as a reference point for determining the ratio, it should have incorporated an ion recombination measurement. This ion recombination factor would be inherited by the calorimeter-derived ion recombination factor. The impact of this is likely to be minimal however, due to the low dose rate at this reference point, and small relative to the large uncertainties.

The high uncertainty of the k_s factor, due to poor quality of fit is likely indicative of the unsuitability of the Jaffé plot method at the extremely high instantaneous dose rate in combination with the large plate separation. Further investigations incorporating measurements of k_s should be completed using an established dose-rate independent detector, such as alanine. Nevertheless, in a clinical environment these methods may not be suitable for a beam monitor due to the long readout processes (taking several days), for which an in-situ calorimeter derived k'_s may be more suitable.

The observed increase in Type A uncertainty of the calorimeter at low dose rates suggests that follow-up measurements are required to investigate its performance further, especially considering the long beam exposure times in clinical or preclinical environments. Additionally, the repeatability and long-term stability of the hybrid dosimeter in maintaining calibration — essential for clinical or preclinical research applications — were not assessed in this study.

This study intentionally omitted Monte Carlo simulations of the incident radiation beam, limiting the scope to finite element modelling of the electrical and thermal behaviour using COMSOL. However, as it was restricted to a single radiation field size and a single beam energy, it is still appropriate to draw conclusions from relative measurements. Future work should incorporate Monte Carlo simulations to enhance the accuracy of the findings, and guide a refined instrument design.

5 Instrument improvements

The dual-calorimeter setup allows for independent operation of the cores, providing redundancy, but it could be configured in a "diagonal bridge" arrangement on opposite sides of the Wheatstone bridge circuit. This configuration effectively doubles the electrical sensitivity while maintaining the same V_{BE}. Given the strong quadratic relationship between self-heating and the parameters discussed in section 3.1.1, this design could be particularly beneficial for reducing the electrical heating of the thermistors, though it may also increase noise levels and will need more evaluation.

Alternatively, to reduce the WET of the device, one calorimeter could be replaced with a thin conductive element, retaining only the primary calorimeter. If this approach is adopted, substituting the calorimeter where HT is applied may reduce the potential for electrical interference and simplify the electronic readout. This would additionally reduce the aluminium attenuation to 0.6 mm, making it comparable with other commercially available beam monitors such as the IBA Stealth, with 0.5 mm thick aluminium attenuation [21].

To improve the performance of the ionisation chamber and reduce the k_s correction factor, the air gap between the proximal and distal calorimeter should be reduced. Published studies indicate that chambers with a 2 mm gap are unsuitable for UHDR dosimetry, whereas reducing the gap to below 1 mm can achieve recombination corrections of less than 5% [28] — a requirement for reference dosimetry under AAPM TG-51. In addition, implementing a guard ring would help maintain a uniform electric field, thereby reducing polarity effects and improving overall chamber stability.

2026 JINST 21 P06001

6 Conclusion

The data presented demonstrate the feasibility of combining an ionisation chamber and a calorimeter into a single instrument for UHDR-RT beam monitoring. However, additional considerations must be addressed to optimise their interaction, as both components significantly influence each other's performance. Many parameters were inherited from their respective components without substantial consideration of how a combined system would behave (e.g., surface-to-surface distance, nominal thermistor resistance, and nominal HT). Future studies must evaluate these parameters to enhance instrument design.

While this work focused on UHDR-RT due to the challenges associated with ionometry at these dose rates, further studies at CONV-RT are essential to validate the clinical performance of the instrument. This research marks the initial steps in developing a hybrid dosimeter that effectively leverages the strengths of both technologies.

In a combined device, users may not need to employ the calorimeters frequently, reserving their use for quality assurance or post-delivery analysis in comparison with log files. Consideration should also be given to how this hybrid device could integrate with existing clinical workflows and systems to enhance its practicality and usability in real-world settings. Seamless integration will facilitate its adoption and ensure that it complements existing dosimetry practices, ultimately benefiting patient care. It is essential to recognise that calorimetry can be complex, and without sufficient training and education, the incorporation of a calorimeter into an ionisation chamber may lead to errors, suggesting that the analysis of the device could benefit from automation.

Overall, this instrument holds significant potential for dose-rate validation, with the capability to reduce uncertainty in UHDR-RT measurements, ultimately enhancing the accuracy and reliability of radiation therapy delivery. Through ionometry, it offers a near-instantaneous response, while calorimetry provides dose-rate independence.

Acknowledgments

This work was partially funded by an Explorer's Award from the National Physical Laboratory's Directors' Science and Engineering Fund. This work was supported by U.K. Research and Innovation (grant MR/Y018761/1). Gratitude is extended to Dr Isaac Halstead for his invaluable assistance in providing training on 3D printing for the resin supports and for generously donating the use of a 3D printer for this project. This collaboration has been instrumental in the success of this work.

Conflict of interest. The Transmission Calorimeter design has been protected under a priority patent application filed in May 2022 [17].

A Contributor Roles Taxonomy (CRediT) author statement [32] is provided in table 3.

2026 JINST 21 P06001

Table 3. Table representing CRediT author statement.

Author	Conceptualisation	Methodology	Software	Validation	Formal Analysis	Investigation	Resources	Data Curation	Writing — Original Draft	Writing — Reviewing & Editing	Visualization	Supervision	Project Administration	Funding acquisition
Samuel Flynn	✗	✗	✗	✗	✗	✗	✗	✗	✗	✗	✗	✗	✗	✗
Rebecca Habgood		✗		✗		✗				✗				
Graham Bass		✗				✗	✗			✗		✗		
Anna Subiel		✗				✗				✗		✗		✗
Russell Thomas		✗				✗				✗				
Iain D.C. Tullis						✗				✗				
Kristoffer Petersson						✗				✗				
Nigel Lee		✗		✗		✗				✗		✗		

References

[1] V. Favaudon et al., *Ultrahigh dose-rate FLASH irradiation increases the differential response between normal and tumor tissue in mice*, *Sci. Transl. Med.* **6** (2014) 245ra93 [*Erratum ibid.* **11** (2019) eaba4525].

[2] B.W. Loo et al., *(P003) Delivery of Ultra-Rapid Flash Radiation Therapy and Demonstration of Normal Tissue Sparing After Abdominal Irradiation of Mice*, *Int. J. Radiat. Oncol. Biol. Phys.* **98** (2017) E16.

[3] P. Montay-Gruel, L. Meziani, C. Yakkala and M.-C. Vozenin, *Expanding the therapeutic index of radiation therapy by normal tissue protection*, *Br. J. Radiol.* **92** (2018) 20180008.

[4] M.-C. Vozenin et al., *The Advantage of FLASH Radiotherapy Confirmed in Mini-pig and Cat-cancer Patients*, *Clin. Cancer Res.* **25** (2019) 35.

[5] E.C. Daugherty et al., *FLASH Radiotherapy for the Treatment of Symptomatic Bone Metastases (FAST-01): Protocol for the First Prospective Feasibility Study*, *JMIR Res. Protoc.* **12** (2023) e41812.

[6] *FLASH Radiotherapy for the Treatment of Symptomatic Bone Metastases in the Thorax (FAST-02*, NCT05524064, Varian, a Siemens Healthineers Company (2025), https://clinicaltrials.gov/study/NCT05524064.

[7] *Irradiation of Melanoma in a Pulse (IMPulse)*, NCT04986696, Centre Hospitalier Universitaire Vaudois (2025) https://clinicaltrials.gov/study/NCT04986696.

[8] *FLASH Radiotherapy for Skin Cancer (LANCE)*, NCT05724875, Centre Hospitalier Universitaire Vaudois (2026), https://clinicaltrials.gov/study/NCT05724875.

[9] *eFLASH for Skin Lesions of Malignant Melanomas (Flash-Skin I)*, NCT06549439, University of Zurich (2025), https://clinicaltrials.gov/study/NCT06549439.

2026 JINST 21 P06001

[10] K. Petersson et al., *High dose-per-pulse electron beam dosimetry — A model to correct for the ion recombination in the Advanced Markus ionization chamber*, *Med. Phys.* **44** (2017) 1157.

[11] M. McManus et al., *The challenge of ionisation chamber dosimetry in ultra-short pulsed high dose-rate Very High Energy Electron beams*, *Sci. Rep.* **10** (2020) 9089.

[12] *Determination of absorbed dose in a patient irradiated by beams of X or gamma rays in radiotherapy procedures*, ICRU report 24, International Commission on Radiation Units and Measurements, Washington, DC, U.S.A. (1987), https://inis.iaea.org/records/ahv8z-s1w87.

[13] A. Lourenço et al., *Absolute dosimetry for FLASH proton pencil beam scanning radiotherapy*, *Sci. Rep.* **13** (2023) 2054.

[14] A. Bourgouin et al., *The probe-format graphite calorimeter, Aerrow, for absolute dosimetry in ultrahigh pulse dose rate electron beams*, *Med. Phys.* **49** (2022) 6635.

[15] G.A. Bass, D.R. Shipley, S.F. Flynn and R.A.S. Thomas, *A prototype low-cost secondary standard calorimeter for reference dosimetry with ultra-high pulse dose rates*, *Br. J. Radiol.* **96** (2022) 20220638.

[16] S. Green et al., *IPEM code of practice for proton therapy dosimetry based on the NPL primary standard proton calorimeter calibration service*, *Phys. Med. Biol.* **70** (2025) 065016.

[17] S.F. Flynn et al., *Transmission calorimeter for measuring dose of radiation*, Patent WO2023227909A1 (2022), https://worldwide.espacenet.com/patent/search/family/082324167/publication/WO2023227909A1?q=WO2023227909.

[18] J.J. Bateman et al., *A novel approach for proton therapy pencil beam scanning patient specific quality assurance using an integrated detector system and 3D dose reconstruction*, *Front. Oncol.* **15** (2025) 1677439.

[19] E. Konradsson et al., *Reconfiguring a Plane-Parallel Transmission Ionization Chamber to Extend the Operating Range into the Ultra-High Dose-per-pulse Regime*, *Radiat. Res.* **201** (2024) 252.

[20] E. Konradsson et al., *Correction for Ion Recombination in a Built-in Monitor Chamber of a Clinical Linear Accelerator at Ultra-High Dose Rates*, *Radiat. Res.* **194** (2020) 580.

[21] J.A. Gersh, *Stereotactic Beam Characterization Using The IBA Stealth Reference Detector*, White paper, IBA Dosimetry (2014), https://www.iba-dosimetry.com/fileadmin/user_upload/products/02_radiation_therapy/StealthChamber/Stereotactic_Beam_Characterization_IBA_Stealth_Reference_Detector_-_Gersh_Whitepaper.pdf.

[22] D. Ceska, *Reference detector for small fields — The T-REF Chamber*, *Med. Phys. Int. J.* **4** (2016) 47.

[23] *FreeCAD: Your own 3D parametric modeler*, https://www.freecad.org/.

[24] M.J. Berger, J.S. Coursey, M.A. Zucker and J. Chang, *Stopping-Power & Range Tables for Electrons, Protons, and Helium Ions*, https://www.nist.gov/pml/stopping-power-range-tables-electrons-protons-and-helium-ions.

[25] COMSOL Multiphysics, *About COMSOL*, https://uk.comsol.com/company.

[26] A. Berne et al., *Monitoring electron energies during FLASH irradiations*, *Phys. Med. Biol.* **66** (2021) 045015.

[27] G. Verona Rinati et al., *Application of a novel diamond detector for commissioning of FLASH radiotherapy electron beams*, *Med. Phys.* **49** (2022) 5513.

[28] F. Gómez et al., *Development of an ultra-thin parallel plate ionization chamber for dosimetry in FLASH radiotherapy*, *Med. Phys.* **49** (2022) 4705.

2026 JINST 21 P06001

[29] J. Cayley et al., *Establishing Linearity of the MOSkin Detector for Ultra-High Dose-per-Pulse, Very-High-Energy Electron Radiotherapy Using Dose-Rate-Corrected EBT-XD Film*, *Appl. Sci.* **15** (2025) 8101.

[30] D. Villoing et al., *Technical note: Proton beam dosimetry at ultra-high dose rates (FLASH): Evaluation of GAFchromic™ (EBT3, EBT-XD) and OrthoChromic (OC-1) film performances*, *Med. Phys.* **49** (2022) 2732.

[31] F. Horst et al., *PP13.06 dosimetric characterization and quality assurance concept for MRI-guided proton therapy with an in-beam MR scanner*, *Phys. Med.* **125** (2024) 103900.

[32] L. Allen, A. O'Connell and V. Kiermer, *How can we ensure visibility and diversity in research contributions? How the Contributor Role Taxonomy (CRediT) is helping the shift from authorship to contributorship*, *Learn. Publ.* **32** (2019) 71.

2026 JINST 21 P06001